Revised Manuscript submitted to: Journal of Physics D: Applied Physics

Microstructure defects mediated charge transport in Nb-doped Epitaxial $BaTiO_3$ thin films

Jian Zhou,[1] Xiaosai Jing,[1] Marin Alexe,[2] Jiyan Dai,[3] Minghui Qin,[1] Sujuan Wu,[1] Min Zeng,[1] Jinwei Gao,[1] Xubing Lu,[1,a)] and J. –M. Liu[1,4,b)]

[1] *Institute for Advanced Materials and Guangdong Provincial Laboratory of Quantum Engineering and Quantum Materials, South China Normal University, Guangzhou, 510006, China*

[2] *Department of Physics, University of Warwick, Coventry CV4 7AL , West Midlands , UK*

[3] *Department of Applied Physics, The Hong Kong Polytechnic University, Hunkom, Hong Kong, China*

[4] *Laboratory of Solid State Microstructures, Nanjing University and Innovation Center of Advanced Microstructures , Nanjing 210093, China*

[Abstract] Nb-doped $BaTiO_3$ (BNTO) films were deposited on MgO substrates at different substrate temperatures by pulsed laser deposition. The temperature dependence of their resistivity, carrier mobility, and carrier concentration were systematically investigated. It reveals that the BNTO films deposited at lower temperature show higher resistivity and lower carrier mobility, and only show semiconductor characteristics at measurement temperatures ranging from 10 K to 400 K. While there is a metal-semiconductor transition at about 20 K for the films grown at relatively higher temperature. The intrinsic mechanism responsible for the different charge transport behavior was revealed by the microstructure studies. Low crystal quality and high density of microstructure defects, observed for BNTO films grown at low temperatures, are particularly affecting massively the charge transport behavior of the BNTO films. This microstructure defects mediated charge transport is dominated by thermal excitation process.

Keywords: $BaTiO_3$; charge transport; microstructure defects; conductivity; carrier mobility

PACS numbers: 77.55.fp; 72.80.Ng; 61.72.-y; 73.50.Gr

[a)] Electronic mail: luxubing@scnu.edu.cn
[b)] Electronic mail: liujm@nju.edu.cn

1. Introduction

$BaTiO_3$ (BTO) is a classical perovskite oxide material with wide potential applications based on its ferroelectricity, piezoelectricity and photo-refractivity.[1, 2] Stoichiometric $BaTiO_3$ is an insulator with a bandgap in the range of 3.2 - 3.4 eV and a resistivity of about 10^{10} Ω·cm. The bandgap is located between a valence band composed primarily of oxygen 2*p* levels and an empty conduction band derived from the titanium 3*d* t_{2g} orbitals.[3, 4] While ferroelectricity of insulating $BaTiO_3$ has been under the focus mainly for applications related to ferroelectric memories, little attentions on the conductivity has been paid, except its unique positive resistivity-temperature coefficient.[5] Recently, great attentions have been paid on the ferroelectric semiconducting oxide materials for their applications in resistive switching memory and photovoltaic solar cells.[6-9]

Insulating $BaTiO_3$ can become conductive either through doping with trivalent rare-earth ions on Ba^{2+} site[10-12] or pentavalent ions on Ti^{4+} site[13] or through reduction ($BaTiO_{3-\delta}$).[14] Many conduction mechanisms spanning from thermal excitation, hopping conduction to polaron conduction have been brought forward to describe charge transport in conductive $BaTiO_3$. In the case of Ti^{4+} site doping, especially the case of Nb doping, considerable effort has been paid to study the electrical transport in BTO bulk or epitaxial films.[13, 15-19] The results obtained show wide discrepancies. Kahn *et al*.[19] point out a variable range hopping conduction mechanism for 2 %at Nb-doped BTO thin film in the range of 150 ºC to 300 ºC. Shao et al.[13] provide an evidence of the small singlet bi-polaron mechanism in their single phase $BaTi_{1-x}Nb_xO_3$ ($0.2 \leq x \leq 0.75$). Liu *et al*.[18] brought evidence of the small polaron conduction mechanism in single phase $BaTi_{1-x}Nb_xO_3$ ($0.01 \leq x \leq 0.5$). The majority of these studies favor small polaron conduction which generality consists of three regimes as discussed by Appel [20] and Klinger.[21] At low temperature, the polarons behave as heavy particles in a band, showing metallic transport behavior. At intermediate temperature, hopping motion dominates the conduction, leading to an activated behavior. Finally, the polaron states are thermal dissociated as the temperature is higher than the activation energy, leading to a thermal activation charge transport behavior.

When compared with $SrTiO_3$ system, which has the similar crystal structure and electronic structure,[22] BTO system exhibits much different charge transport behaviors. For

example, the reported carrier mobility value is much lower than that of the STO system. For La-doped STO epitaxial films, the carrier mobility can reach as high as 32,667$cm^2/V{\cdot}s$.[23] However, for single crystal BTO the reported carrier mobility is usually below 1.0 $cm^2/V{\cdot}s$ and the reported highest value is only 15 $cm^2/V{\cdot}s$.[12, 24] Another noticeable difference is that the conductivity of the STO system can be easily transformed among insulator-semiconductor-metallic behaviors, whereas for BTO system it is not easy to obtain very high conductivity or metallic transport. The bulk BTO has always a critical doping point. That is the conductivity increases with the doping concentration of the dopants, and it will decrease again above a certain doping concentration. Moreover for BTO films situation is even more complicated. For instance, MOCVD-grown BTO films show similar critical doping phenomena, while this critical doping concentration disappears for films deposited by pulsed laser deposition (PLD). The above mentioned charge transport behavior suggests that the charge transport behaviors of BTO system and corresponding intrinsic mechanisms need to be further investigated, which will be very important for potential applications such as photovoltaic and resistive switching memory.

In the past, most of the studies [13, 15-18, 25] focused on the effect of chemistry defects on the conductivity and charge transport behaviors of BTO. Unfortunately, studies on the effect of microstructure on the conductivity of BTO, especially for thin films, are rather limited.[13, 26] In this work we focuses on the less explored effect of microstructure defects on the conductivity and charge transport behaviors of BTO. We targeted different microstructures by depositing the BTO films by PLD at various temperatures and we have been able to show that the conductivity and charge transport can be significantly tuned by the microstructure defects.

2. Experimental Details

$BaNb_{0.5}Ti_{0.5}O_3$ (BNTO) films were deposited on MgO (001) single crystal substrate using pulse laser deposition (PLD) technique. The Nb doping concentration of 50 %at was chosen in this work is to obtain reliable Hall Effect measurement results at low temperature. MgO substrate was chosen is to avoid the interfacial oxygen vacancy diffusion effect which was always found to play a critical role on the conductivity and charge transport for BTO deposited on $SrTiO_3$ (STO) substrate. The details on the Nb-doping concentration effect and

interface oxygen vacancy diffusion effect on the BTO/STO structure will be discussed in our other work. BNTO thin films with thickness of ~80 nm were grown in a temperature range from 500 ºC to 700 ºC and at an oxygen ambient pressure of 3.0×10^{-4} Pa. A polycrystalline $BaNb_{0.5}Ti_{0.5}O_3$ ceramic pellet (Goodwill) was used as ablation target. During the deposition, a KrF excimer laser with a wavelength of 248 nm was operated at 3 Hz and the laser fluence was fixed to 1.0 J/cm^2. After the deposition, the films were cooled down in vacuum to avoid the compensation of oxygen. X-ray diffraction (XRD) analyses were carried out using a PANalytical X'Pert Pro diffractometer with Cu K_α radiation (λ=1.5406Å). The surface morphology of the samples was investigated using a Cypher Asylum Research atomic force microscope (AFM). A JEOL JEM2100F high resolution transmission electron microscope (HRTEM), with point resolution of 0.194 nm and working voltages of 200 kV, was used to carry out cross-section analysis and selected area electron diffraction (SAED) measurement. The cross-sectional and planar view specimens for transmission electron microscopy (TEM) observation were prepared by the conventional processes of slicing, grinding and finally ion-milling. The temperature dependence of the resistivity and Hall Effect measurements were performed by van der Pauw method using a physical property measurement system (PPMS 9, Quantum Design).

3. Results and Discussion

Figure 1 (a) shows the 2θ/θ scans of samples grown at temperature of 500 ºC, 550 ºC, 600 ºC, 650 ºC and 700 ºC. From the figure, (001) peaks of BNTO with no other diffraction peaks originate from impurity phase can be clearly observed for all the samples. (002) and (003) peaks can be observed only for the films grown at 700 ºC. The disappearance of (002) peaks for these films grown below 700 ºC is most probably due that their out of plane lattice constant is very close to that of MgO substrate. The (002) diffraction peaks for BNTO films are hard to distinguish from the diffraction peak of MgO substrate. Another possible reason for the disappearance of (002) and (003) peaks is that the crystallinity of the BNTO films is not good enough to get clear diffraction peaks for films grown below 700 ºC. Figure 1(b) especially shows the diffraction patterns for (001) peaks. The (001) peaks shown in Figure 1(b) revealed a clear shift to the larger angles for the 700 ºC grown sample compared with that of the other four samples. Correspondingly, the out of plane lattice constant shrinks from

4.162 Å to 4.135 Å. The absolute diffraction intensity of (001) peak increases with the increase of growth temperature and the full width at half maximum (FWHM) values decreases with the increase of the growth temperature, both of which imply an enhancement of crystal quality with increase of deposition temperature. In addition to 700 ºC grown sample, the other four samples exhibit no clear shifts of the (001) peaks, which implies that the low temperature below 700 ºC didn't bring clear effects on their out of plane lattice constants. The surface morphologies measured by AFM revealed a slight increase of the surface roughness with the increase of the growth temperature.

Figure 2 shows the typical AFM surface morphology images of the samples grown at different temperatures. Very flat surfaces have been observed for all of these samples. For films with ~80-100nm physical thickness, their surface root of mean square（RMS）is as small as ~ 0.2 nm. Another feature shown in Fig. 2 is that growth temperature didn't affect significantly on their surface roughness. All the RMS values are between 0.1 nm and 0. 2nm. The microstructures of three representative BNTO films grown at 500 ºC, 600 ºC, and 700 ºC were studied by cross-sectional TEM along the [010] crystal direction.. Figures 3 (a), (b), and (c) show the low- magnification TEM images of the three samples. Clear interface between MgO substrate and BNTO film can be observed, and the film thicknesses are determined to be ~80 nm. Figures 3 (d), (e), and (f) show the high-resolution TEM images of the same samples. The main difference among the TEM images is that the 700 ºC grown film shows more perfect crystal structure compared to the other two films. The epitaxial quality increases with the increase of the growth temperature. In 500 ºC grown film, some amorphous and disordered structures can be clearly seen.

Figure 4(a) shows the temperature dependent resistivity characteristics of the BNTO films. The dc resistivity of BNTO films shows a clear dependence on the growth temperature. Sample grown at 500 ºC exhibits the highest resistivity during the whole measurement temperature range. The resistivity gradually deceases with the increase of the growth temperature. Films deposited at low temperatures of 500 ºC and 550 ºC show semiconductor transport behaviors spanning the whole range of measurement temperature (10K-400K). For films grown at 600 ºC, 650 ºC, and 700 ºC, the resistivity exhibits entirely the semiconductor transport behaviors. However, a metal-semiconductor-like transition occurs at a low

temperature of around 20 K. When the temperature is lower than 20 K, the transport behaviors of the three samples are metallic like, as shown in Figure 4(b). This low temperature metal-semiconductor transition has been also observed in the $BaTi_{0.8}Nb_{0.2}O_3$ ceramics, which implies a crossover from band to hopping transport of the charge carriers.[27] In the work done by Shao et al.[13] and Liu et al.[18], the charge transport behaviors of the BNTO films exhibit to be either semiconductor or metal behaviors in the whole temperature range depending on the Nb-doping concentration.

Figure 5(a) shows the temperature dependent Hall coefficient R_H for all of the Nb-doped BTO films. The negative Hall coefficient indicates the majority of carriers in the BNTO films are electrons. The Hall coefficient shows obvious temperature dependence for all of the samples. The absolute values of R_H decreases with the increase of measurement temperature. The different temperature behaviors of Hall coefficient implies that the microstructures, which is controlled by the growth temperature, plays an important role on their charge transport behaviors of BNTO films. Figure 5(b) shows temperature dependence of carrier concentration, which is calculated according to the formula: $R_H = 1/en$. Similar to R_H, the carrier concentration also exhibits a slight temperature dependence. Unlike R_H, the carrier concentration increases with the increase of the measurement temperature, which implies that the thermal excitation may dominate the movement of the carriers. It is demonstrated that the carrier is localized in the defect energy levels at low temperature. At higher temperature localized carriers will be excited to the conduction band leading to the increase of the carrier density. The overall carrier concentration is in the $\sim 10^{21}$ cm^{-3} , which is similar to the reported values[18]. Figure 5(c) shows the temperature dependence of the carrier mobility as a function of growth temperature. The mobility does not show a significant variation on the entire temperature range. Only a slight increase of the carrier mobility at high temperatures can be observed. The most noticeable results shown in Figure 3(c) is that low temperature grown films of 500 ºC and 550 ºC exhibits a clear smaller mobility than that of the films grown at high growth temperature above 550 ºC. It has been shown that the carrier scattering in the semiconductors is dominated by phonon scattering and impurity scattering[13]. The temperature stability of carrier mobility in the present BNTO films suggests that the phonon scattering may not be the important scattering factor. The clear mobility difference between

high and low grown temperature samples implies that the impurity scattering, which is most probably induced by the microstructure defects, prevails the charge transport in the BNTO films.

From Figure 5, it should be noticed that the carrier mobility as well as carrier concentration and hall coefficient does not strictly changes with the change of BNTO film growth temperatures. For films grown at 500℃,600℃, and 700℃, the carrier concentration and carrier mobility increases exactly with the increase of the growth temperature, while the absolute value of hall coefficient decreases with the increase of the growth temperature. Considering the XRD and cross-sectional TEM results, these carrier transport characteristics exhibit a direct relationship with their film microstructures. For films grown at 550℃ and 650℃, their carrier transport characteristics somewhat deviate from the changing tendency of the other three samples. The reason is still not very clear now. We assume that the chemical defects like cation vacancy or oxygen vacancy may also work on the films' charge transport. For example, cation vacancy will trap free electron, and it will directly affect the carrier concentration and hall coefficient. In our experiment, except for the growth temperature, the growth parameters for BNTO films are assumed to be nearly same. However we still can't exclude the existence of the differences in the chemical defect density (like cation vacancy and oxygen vacancy) in the film. Therefore we observe some fluctuation of the carrier concentration, carrier mobility etc. Further work will be carried out to clarify the complex charge transport mechanism in BNTO films. From Figure 4 and 5, we can also learn that a growth temperature around 650℃ should be a suitable temperature parameter to get comparatively low resistivity and high carrier mobility for BNTO films.

We analyzed the charge transport mechanisms further by fitting the resistance-temperature (R-T) using various charge transport models. The small polaron hopping and variable range hopping models do not reasonably fit the data for all the five samples. The R-T curves at some specified temperature range can be well fitted by using the thermal activation models, which is expressed as follows:

$$\rho = \rho_0 \exp(E_a/k_B T) \qquad (1)$$

where E_a is the activation energy, k_B is Boltzman's constant. The Arrhenius plot from Figure

6(a) for films grown at low temperatures like 500 ºC and 550 ºC, the fit is good only at temperatures higher than 200 K, while the films grown above 550 ºC, the fitting range can extend down to about 100 K. The activation energy is shown in Figure 6(b). The overall activation energy are around ~ 20 meV or smaller, suggesting that the electrons provided by oxygen vacancies or doped Nb^{5+} are localized at a comparatively shallow energy levels in the forbidden gap. The activation energy also shows a strong dependence on the growth temperature, which decreases as the increase of growth temperature. Except for growth temperatures, other growth parameters are same for all these samples, the only possible mechanisms to affect the difference of the activation energies is the film microstructures controlled by their growth temperatures.

To further confirm the above proposed influence of the microstructure, we carried out the HRTEM investigations. Figure 7(a) and (b) show the planar-view TEM images of samples grown at 500 ºC and 700 ºC, respectively. The sample grown at 500 ºC exhibits a rather disordered crystal structure, in which many defects and large grain boundaries can be seen clearly. Polycrystalline phase and even amorphous phase coexist, and grain boundaries can be clearly found. Rising the growth temperature to 700 ºC improve massively the crystallinity and film quality, as can be seen in Figure 7(b). The density of grain boundaries and defects were greatly reduced. The HRTEM images in the insets of Figure 7(a) and (b) show amorphous and grain boundaries for 500 ºC grown sample and near perfect lattice for 700 ºC grown sample. The microstructure and defects are further confirmed by selected area electron diffraction (SAED) as shown in Figure 7(c) and (d). The dotted spots and circles observed in the SAED patterns imply the amorphous and multi-crystalline structure in the 500 ºC grown BNTO film. On the contrary, the stream-line patterns in the SAED images proved the single crystal growth structure of the 700 ºC grown BNTO sample. Since all the growth parameters of all the five BNTO films are same except the growth temperatures, the differences of resistance, carrier mobility, Hall coefficients implies that the microstructure defects controlled by the growth temperature is one of the critical mechanisms affecting the charge transport behavior. It provides new insights to clarify the big differences of charge transport behaviors between BTO system and STO system. At least the imperfect epitaxial quality should be one of the reasons leading to the low carrier mobility of BTO system, although the carrier

scattering effect due to the dipoles in BTO can't be excluded.

4. Conclusion

In summary, we made a systematical investigation on the charge transport behaviors of the Nb-doped BTO films. The BNTO films deposited at different temperatures shows clearly different charge transport behaviors. The mechanisms affecting the charge transport are mainly related to the film microstructure，which is significantly affected by their growth temperatures. Generally low temperature grown films have a low crystallinity and high defect density, while at high temperatures the films show good epitaxial quality with lower defect density. The films grown at ~650 ºC shows a higher carrier mobility and conductivity compared to films grown at other temperatures. This microstructure defects mediated charge transport is dominated by thermal activation process during the main measurement temperature range and the conductivity and charge transport of BTO films can be significantly tuned by the microstructure defects. In addition to widely studied chemical defects, our work proved that physical microstructure defect is another important mechanism to affect the conductivity and charge transport in $BaTiO_3$ films. Our work will deepen the understanding on the complex charge transport mechanisms in BTO films and will be beneficial to their future resistive memory and photovoltaic applications.

Acknowledgement:

This work was supported by the National Natural Science Foundation of China (Contract Nos. 51472093, 51431006, 61271127) and the program for Changjiang Scholars and Innovative Research Team in University (Grant No. IRT1243). M.A. acknowledges the support of Royal Society via Wolfson Award. J.Y.D. thanks the financial support from Hong Kong GRF grant (PolyU514512) and The Hong Kong Polytechnic University's Strategic Importance Grants (1-ZE25 and 1-ZVCG). X.B.L acknowledges the support of Science and Technology Planning Project of Guangdong Province (No.2014B090915004).

Reference

[1] Sayer M, Sreenivas K. 1990 *Science* **247** 1056

[2] Cohen RE. 1992 *Nature* **358** 136

[3] Hudson LT, Kurtz RL, Robey SW, Temple D, Stockbauer RL. 1993 *Phys.Rev.B* **47** 1174

[4] Cox PA. Transition metal oxides: an introduction to their electronic structure and properties: OUP Oxford; 2010.

[5] Yoo H-I, Song C-R, Lee D-K. 2002 *J. Electroceram.* **8** 5-36

[6] Jiang AQ, Wang C, Jin KJ, Liu XB, Scott JF, Hwang CS, Tang TA, Lu HB, Yang GZ. 2011 *Adv. Mater.* **23** 1277

[7] Pantel D, Goetze S, Hesse D, Alexe M. 2012 *Nat.Mater.* **11** 289

[8] Li H, Jin K, Yang S, Wang J, He M, Luo B, Wang J, Chen C, Wu T. 2012 *J. Appl. Phys.* **112** 083506

[9] Ukai Y, Yamazaki S, Kawae T, Morimoto A. 2012 *Jpn. J. Appl. Phys.* **51** 09LE10

[10] Tennery VJ, Cook RL. 1961 *J. Am. Ceram. Soc.* **44** 187

[11] Gilbert SR, Wills LA, Wessels BW, Schindler JL, Thomas JA, Kannewurf CR. 1996 *J. Appl. Phys.* **80** 969

[12] Kolodiazhnyi T, Petric A, Niewczas M, Bridges C, Safa-Sefat A, Greedan JE. 2003 *Phys.Rev.B* **68** 085205

[13] Shao Y, Hughes RA, Dabkowski A, Radtke G, Gong WH, Preston JS, Botton GA. 2008 *Appl.Phys.Lett.* **93** 192114

[14] Kolodiazhnyi T. 2008 *Phys.Rev.B* **78** 045107

[15] Nagano D, Funakubo H, Shinozaki K, Mizutani N. 1998 *Appl.Phys.Lett.* **72** 2017

[16] Yoon S-H, Kim H. 2002 *J. Appl. Phys.* **92** 1039

[17] Lemée N, Dubourdieu C, Delabouglise G, Sénateur J, Laroudie F. 2002 *J. Cryst. Growth* **235** 347

[18] Liu L, Guo H, Lü H, Dai S, Cheng B, Chen Z. 2005 *J. Appl. Phys.* **97** 054102

[19] Nasir Khan M, Kim H-T, Kusawake T, Kudo H, Ohshima K, Uwe H. 1999 *J. Appl. Phys.* **86** 2307

[20] Appel J. Polarons. In: Seitz. F T.D.a.E.H., editor. Solid State Physics. 21. New York: Academic; 1968.

[21] Klinger MI. Problems of Linear Electron (Polaron) Transport Theory in Semiconductors: International Series in Natural Philosophy: Elsevier; 2013.

[22] Hwang J, Kolodiazhnyi T, Yang J, Couillard M. 2010 *Phys.Rev.B* **82** 214109

[23] Son J, Moetakef P, Jalan B, Bierwagen O, Wright NJ, Engel-Herbert R, Stemmer S. 2010 *Nat.Mater.* **9** 482

[24] Yoo H-I, Song C-R, Lee D-K. 2004 *J. Eur. Ceram. Soc.* **24** 1259

[25] Chan HM, Harmer MR, Smyth DM. 1986 *J. Am. Ceram. Soc.* **1986** 69, 507-10

[26] Kim YH, Lu X, Diegel M, Mattheis R, Hesse D, Alexe M. 2013 *J. Adv. Dielectr.* **3** 1350009

[27] Kolodiazhnyi T, Wimbush S. 2006 *Phys.Rev.Lett.* **96** 246404

Figure captions

Figure 1 (Color online) (a) XRD 2θ/θ scan patterns of thin films grown at 500 ºC, 550 ºC, 600 ºC, 650 ºC, 700 ºC; (b) XRD 2θ/θ scan patterns for BNTO (001) peaks.

Figure 2 (Color online) AFM images of BNTO films grown at different temperatures. The right down figure shows a summary of the RSM values dependence on the growth temperature.

Figure 3 (Color online) The cross-sectional TEM lattice images in the vicinity of the BNTO-MgO interfaces along [010] crystal direction. Low-magnification images: (a) 500 ºC; (b) 600 ºC; (c) 700 ºC. HRTEM images: (d) 500 ºC; (e) 600 ºC; (f) 700 ºC.

Figure 4 (Color online) (a) Temperature dependence of resistivity as a function of growth temperature ranging from 500 ºC to 700 ºC; (b) Temperature dependence of resistivity for films deposited at 600 ºC, 650 ºC, 700 ºC between 10 K and 100 K, demonstrating a metal-semiconductor transition.

Figure 5 (Color online) Temperature dependence of (a) Hall coefficient; (b) carrier concentration; and (c) Hall mobility as a function of growth temperature.

Figure 6 (Color online) (a) Arrhenius plot for BNTO films grown at 500 ºC, 550 ºC, 600 ºC, 650 ºC, 700 ºC; (b) activation energy determined from (a) as a function of growth temperature.

Figure 7 Planar-view TEM images of BNTO films grown at 500 ºC (a); and 700 ºC (b), the inset of Figure 5(a) and (b) shows the HRTEM images of the planar TEM observation of 500

ºC and 700 ºC grown films, respectively; the SAED patterns of BNTO films grown at 500 ºC (c); and 700 ºC (d).

Figures

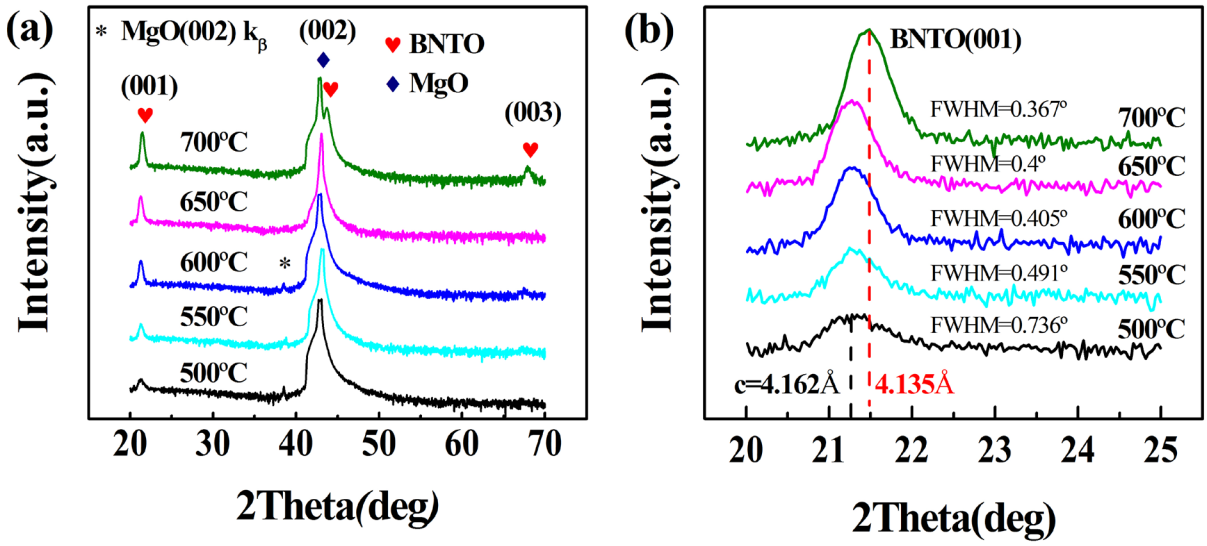

Figure 1 (Color online) (a) XRD 2θ/θ scan patterns of thin films grown at 500 ºC, 550 ºC, 600 ºC, 650 ºC, 700 ºC; (b) XRD 2θ/θ scan patterns for BNTO (001) peaks.

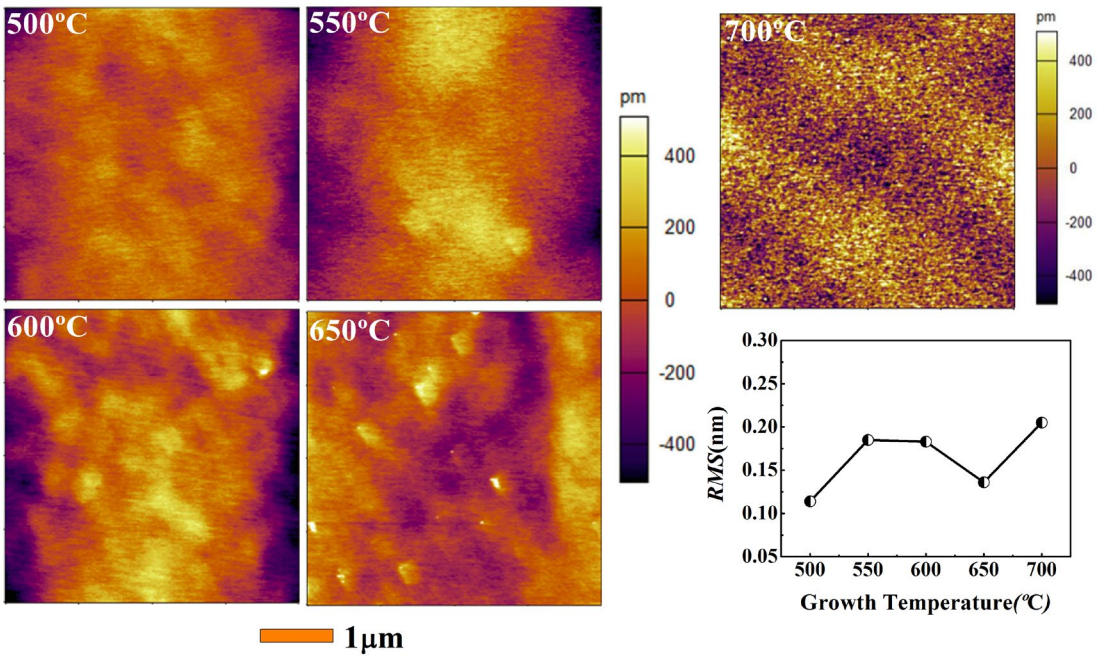

Figure 2 (Color online) AFM images of BNTO films grown at different temperatures. The right down figure shows a summary of the RSM values dependence on the growth temperature.

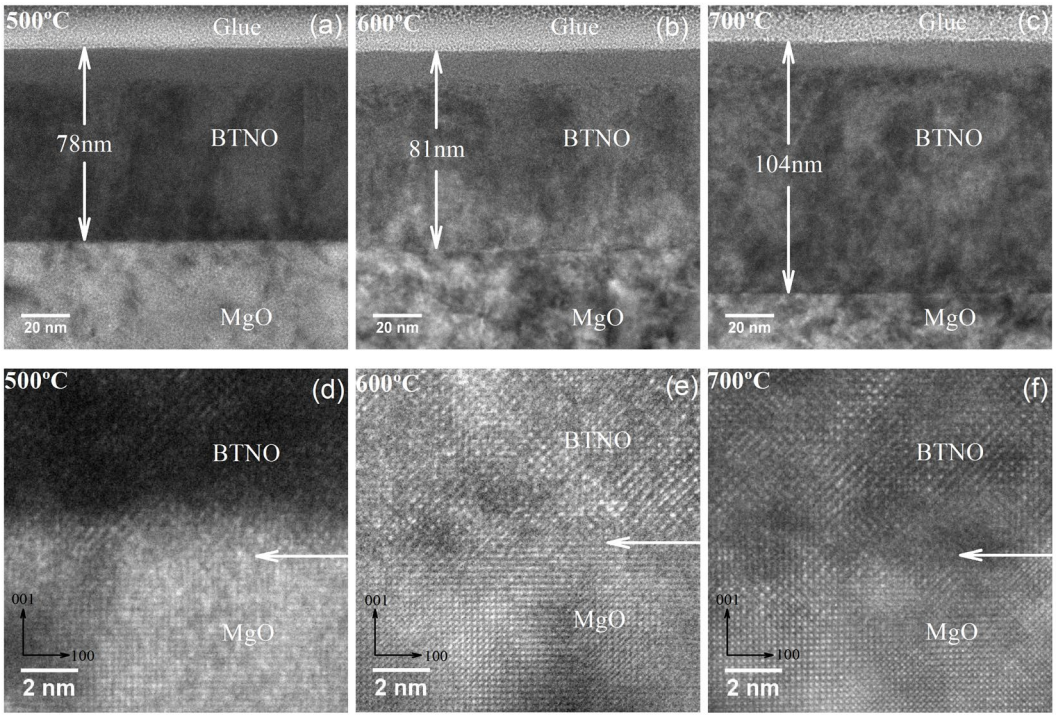

Figure 3 (Color online) The cross-sectional TEM lattice images in the vicinity of the BNTO-MgO interfaces along [010] crystal direction. Low-magnification images: (a) 500 ºC; (b) 600 ºC; (c) 700 ºC. HRTEM images: (d) 500 ºC; (e) 600 ºC; (f) 700 ºC.

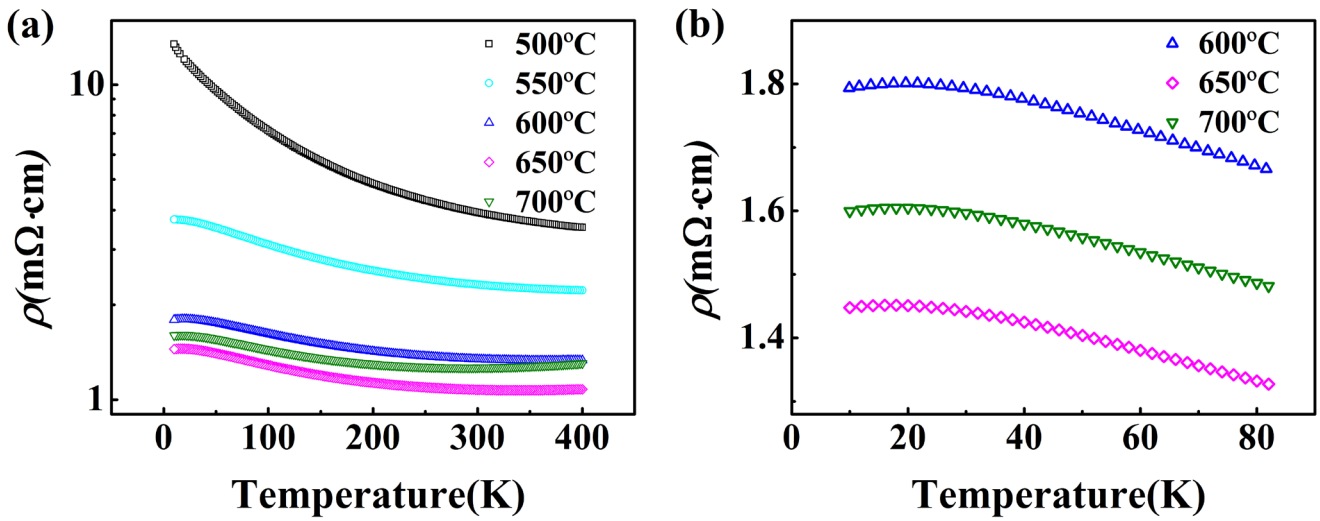

Figure 4 (Color online) (a) Temperature dependence of resistivity as a function of growth temperature ranging from 500 ºC to 700 ºC; (b) Temperature dependence of resistivity for films deposited at 600 ºC, 650 ºC, 700 ºC between 10 K and 100 K, demonstrating a metal-semiconductor transition.

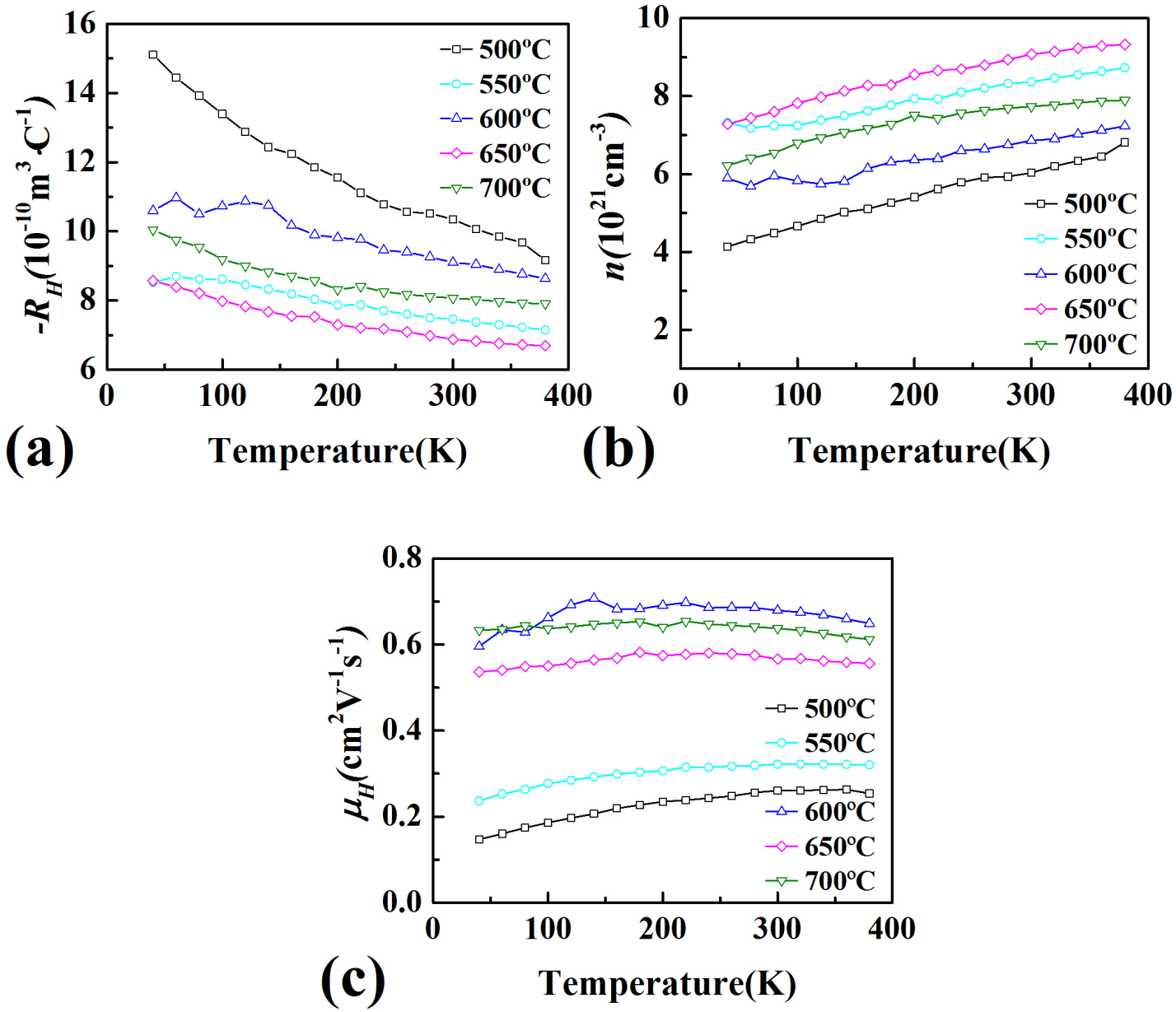

Figure 5 (Color online) Temperature dependence of (a) Hall coefficient; (b) carrier concentration; and (c) Hall mobility as a function of growth temperature.

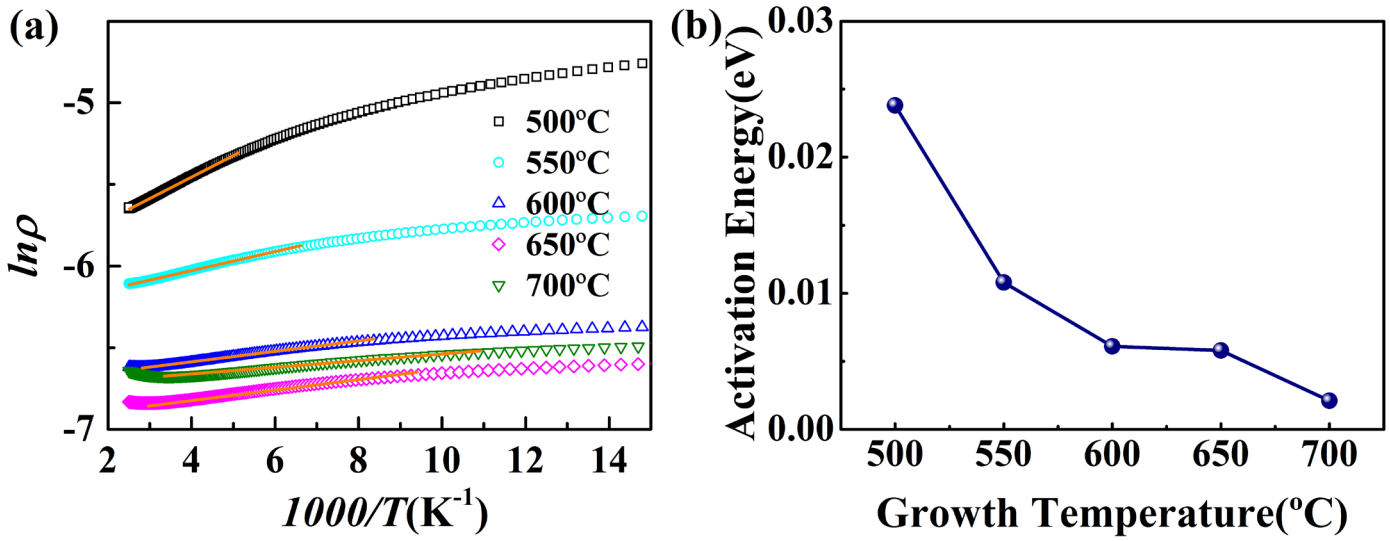

Figure 6 (Color online) (a) Arrhenius plot for BNTO films grown at 500 ºC, 550 ºC, 600 ºC, 650 ºC, 700 ºC; (b) activation energy determined from (a) as a function of growth temperature.

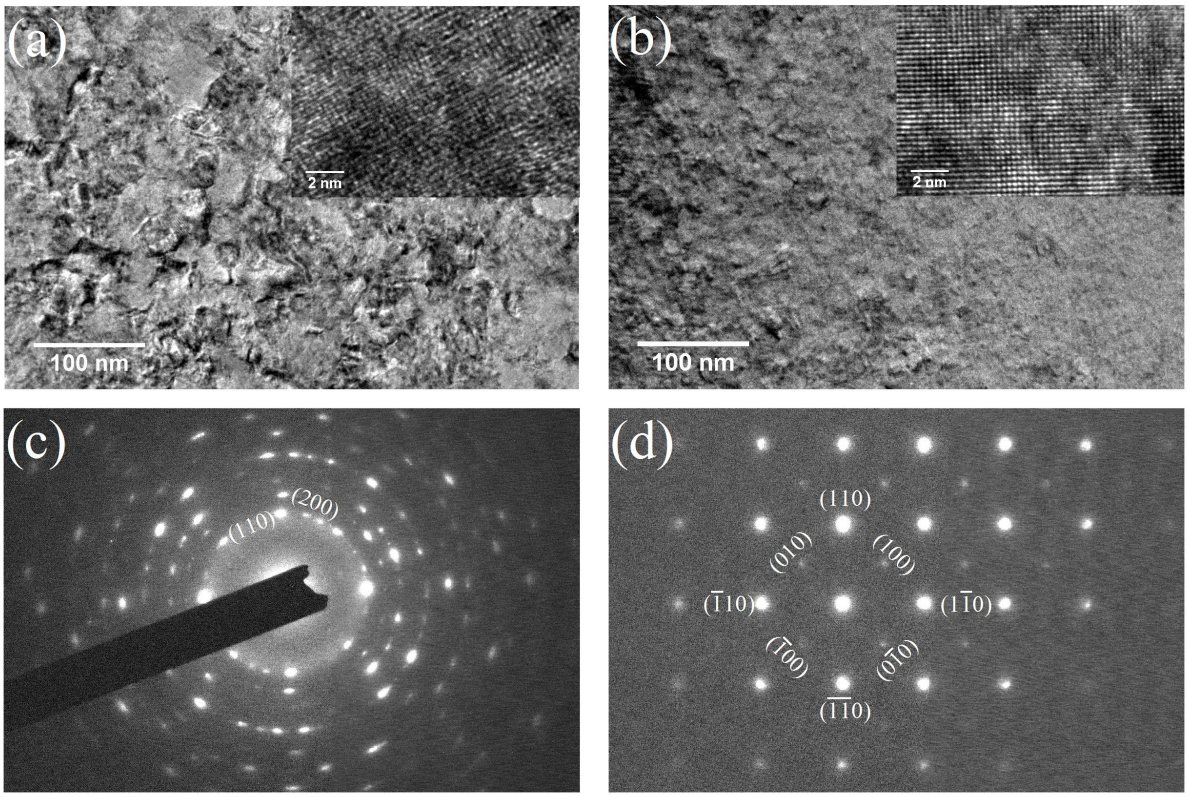

Figure 7 Planar-view TEM images of BNTO films grown at 500 ºC (a); and 700 ºC (b), the inset of Figure 5(a) and (b) shows the HRTEM images of the planar TEM observation of 500 ºC and 700 ºC grown films, respectively; the SAED patterns of BNTO films grown at 500 ºC (c); and 700 ºC (d).